Photonic Color Filters Integrated with Organic Solar Cells for Energy Harvesting

Hui Joon Park,[†,§] Ting Xu,[‡,∥,§] Jae Yong Lee,[‡] Abram Ledbetter,[⊥] and L. Jay Guo[†,‡,⊥,]*

[†]Macromolecular Science and Engineering, [‡]Electrical Engineering and Computer Science, [⊥]Applied Physics, The University of Michigan, Ann Arbor, Michigan 48109, United States, and [∥]Institute of Optics and Electronics, Chinese Academy of Sciences, Chengdu, 610209, China. [§]These authors contributed equally to this work.

Energy efficiency is becoming ever more important for a green and sustainable future. As global energy demand continues to grow to meet the needs and aspirations of people across the world, ways to improve energy efficiency and harvest energy are essential. Recently, a number of approaches have been explored to scavenge energy from the environment, such as photovoltaic (PV),[1] thermoelectric,[2] and piezoelectric effects.[3] However, little attention has been paid to the significant light energy wasted in displays used in our everyday lives. For example, in prevailing liquid crystal displays (LCD), only 3−8% of the backlight can reach our eyes, where most of light energy is absorbed by the colorant-based filters and polarizers.[4] Therefore, approaches that can recycle or harvest the absorbed energy to generate useful electrical power could lead to revolutionary energy-saving e-media. This aspect is especially promising when considering widely used devices such as e-books, which consume little power, or mobile devices (such as cell phones), which are in standby mode 95% of the time. In this paper, we exploit a dual-function photovoltaic color filter device that can produce desirable reflection colors and simultaneously convert the absorbed light to electricity. Such dual functionality can also be exploited to make colored organic photovoltaic (OPV) panels for both decoration and light energy harvesting.

The control of light interaction with nanostructures and their unique applications in photonics have been highlighted in the past decade with the development of nanofabrication and characterization techniques for light management.[5−9] Optical resonance effects in nanoholes,[10,11] nanoslits,[12−14] and related nanostructures[15−18] have been exploited for color filter applications. Here we will use organic semiconductors as an integral part of a specially designed photonic color filter for energy conversion. As a proof of principle, we will demonstrate a reflectance-type color filtering device capable of power generation. Reflective colors are superior to transmissive filter technologies[10−14] for outdoor usage and can work under direct sunlight for more energy absorption and energy conversion using the scheme discussed in this paper. Our conceptual devices recycle the wasted energy in most display applications that require color filters to achieve desirable colors and do not apply to colored displays using emissive devices such as organic light-emitting diode (OLED). Furthermore, we adopt OPV cell structures for our dual-function devices. Therefore, the approach also takes advantage of the OPV, such as low cost, easy fabrication, and compatibility with flexible substrates over a large area.[19−24] In addition, this work points out alternative applications of OPVs, which complements the great efforts in improving its power conversion efficiency (PCE)[20−22] and practical fabrication methods.[21,24]

RESULTS AND DISCUSSION

Since reflectance-type color filters act similarly to color paint, i.e., absorbing light

ABSTRACT Color filters are indispensable in most color display applications. In most cases, they are chemical pigment-based filters, which produce a particular color by absorbing its complementary color, and the absorbed energy is totally wasted. If the absorbed and wasted energy can be utilized, e.g., to generate electricity, innovative energy-efficient electronic media could be envisioned. Here we show photonic nanostructures incorporated with photovoltaics capable of producing desirable colors in the visible band and utilize the absorbed light to simultaneously generate electrical powers. In contrast to the traditional colorant-based filters, these devices offer great advantages for electro-optic applications.

KEYWORDS: solar cell · display · color filter · dual function · photonic nanostructure
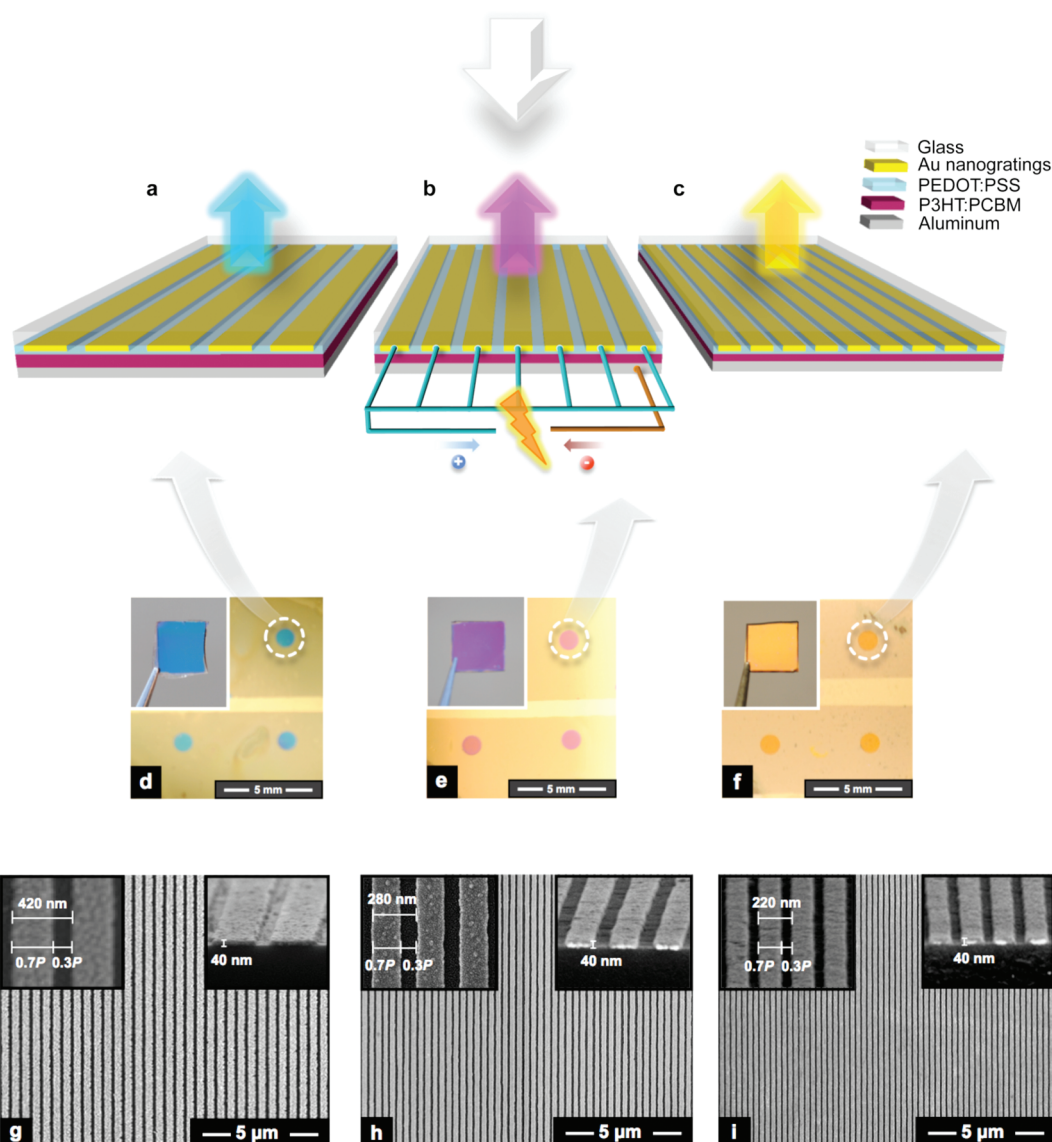
Figure 1. Energy-generating photonic color filters. (a–c) Schematic of dual-function devices. In all three cases, the thicknesses of the Au nanogratings and PEDOT:PSS layer are 40 and 30 nm, respectively. Au nanogratings have a 0.7 duty cycle (Au line width is 0.7 of the period). The photovoltaic property is schematically described in (b) as a representative. (a) Cyan-colored device having 420 nm period Au nanogratings and 90 nm thick P3HT:PCBM photoactive layer. (b) Magenta-colored device having 280 nm period Au nanogratings and a 65 nm thick photoactive layer. (c) Yellow-colored device having 220 nm period Au nanogratings and a 50 nm thick photoactive layer. **(d–f)** Photographs of dual-function devices having a 1 mm diameter circular shape. The inset images are the large-area version having about 1 cm size: (d) cyan, (e) mgenta, and (f) yllow. **(g–i)** Scanning electron microscope (SEM) images of Au nanogratings. The left and right inset images are the high-magnification top and tilted views, respectively. The *P* in the left inset image represents the period of Au nanogratings: (g) 420 nm period, (h) 280 nm period, (i) 220 nm period.

corresponding to specific wavelengths but reflecting the others, here we focus on the CMY color scheme where cyan, magenta, and yellow are the three primary colors. Figure 1a–c present the schematic diagram of the proposed energy-harvesting color filters, where the conjugated polymer layers composed of poly(3, 4-ethylenedioxythiophene):poly(styrenesulfonate) (PEDOT:PSS) and poly(3-hexylthiophene):[6,6]-phenyl C_{61} butyric acid methyl ester (P3HT:PCBM) are sandwiched by an Au nanograting layer and a continuous thick Al film. The selection of each material and its role will be further explained later. Large area metallic nanostructures

can be applicable to semitransparent electrodes for organic optoelectronics by controlling their optical transparency and electrical conductivity.[25,26] Accordingly, the key concept in our design is that the periodic Au nanogratings in the device act not only as nanostructures to modulate the incident light to generate different colors but also as semitransparent anodes for OPV cells. In this structure the low work function Al film acts as a cathode.

Color filters are desired to be polarization insensitive to the incident light. To achieve this, we used different design strategies for the transverse electric (TE) and transverse magnetic (TM) waves so that similar
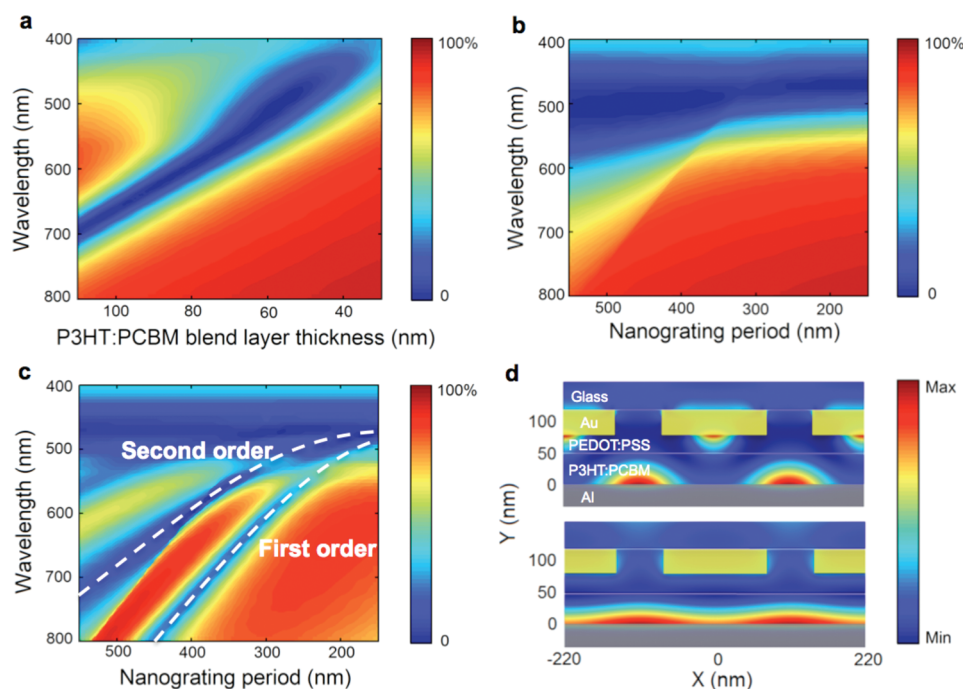
Figure 2. Calculated maps of the reflection for the proposed structures. The thickness of the Au nanogratings and PEDOT:PSS layer are fixed at 40 and 30 nm, respectively. Au nanogratings have a 0.7 duty cycle. (a, b) Reflection for TE polarized waves as a function of (a) the thickness of the P3HT:PCBM blend photoactive layer (Au nanograting period is fixed at 280 nm) and (b) Au nanograting period (the thickness of the photoactive layer is fixed at 50 nm). (c) Reflection for TM polarized waves as a function of Au nanograting period (the thickness of the photoactive layer is fixed at 50 nm). (d) Magnetic field intensity distribution for TM (top) and TE (bottom) waves at the same resonant absorption wavelength of 490 nm. The thickness of the photoactive layer and the period of Au nanogratings are 50 and 220 nm, respectively.

reflection spectra for both polarizations can be obtained for each color. First of all, the structure resembles a Fabry−Pérot cavity. When the light impinges on the Au nanogratings, it will interfere with the waves reflected from the bottom Al film. When destructive interference occurs, the reflection spectra will reach a minimum, the light energy of the corresponding color will be absorbed, and the complementary color will be reflected by the structure. Figure 2a and b show the calculated reflection spectra maps for TE polarized light (the E-field is parallel to the Au nanogra ting direction) as a function of P3HT:PCBM blend layer thickness (Figure 2a, Au grating period fixed at 280 nm) and as a function of Au nanograting period (Figure 2b, blend layer thickness fixed at 50 nm), respectively. The blue regions in these maps represent the reflection minima where the light energy is absorbed by the structure. As expected from the Fabry−Pérot interference, the resonant absorption wavelength is linearly proportional to the thickness of the blend layer but almost independent of the nanograting period. For TM waves (the E-field is perpendicular to the Au nanograting direction), additional consideration needs to be taken, as it is well known that TM waves can be efficiently coupled to the surface plasmon (SP) modes through the subwavelength grating structures.[7,8] Figure 2c gives the calculated map of reflection spectrum for TM polarized waves as a

function of Au nanograting period. Here the P3HT:PCBM blend layer thickness remains 50 nm. In addition to the absorption band produced by the Fabry−Pérot interference, there are two more resonant absorption stripes (marked with white dashed lines) that originate from the splitting of SP modes in the plasmonic waveguide structures.[27,28] The dispersion characteristics of these modes show strong dependence on the Au nanograting period because it provides the phase matching condition for the TM polarized light to couple to the SP mode. We can take advantage of the insensitivity of the Fabry−Pérot resonance to the Au nanograting period and choose a particular period so that the TM polarized light is absorbed around the same wavelength as the TE polarized light, thereby producing polarization-independent reflection colors. Figure 2d shows the simulated magnetic field intensity for TM and TE waves at the same resonant absorption wavelength of 490 nm. The thickness of the P3HT:PCBM blend layer and the periodicity of the Au nanogratings are 50 and 220 nm, respectively. It can be clearly seen that the field distribution for TM polarization exhibits obvious plasmon behaviors at the Au-PEDOT:PSS and Al-P3HT:PCBM interfaces. For the TE polarization, the field distribution resembles that of the conventional Fabry−Pérot interference, further supporting our design principle.

Figure 1g−i show the scanning electron microscope (SEM) images of the fabricated Au nanogratings. Here
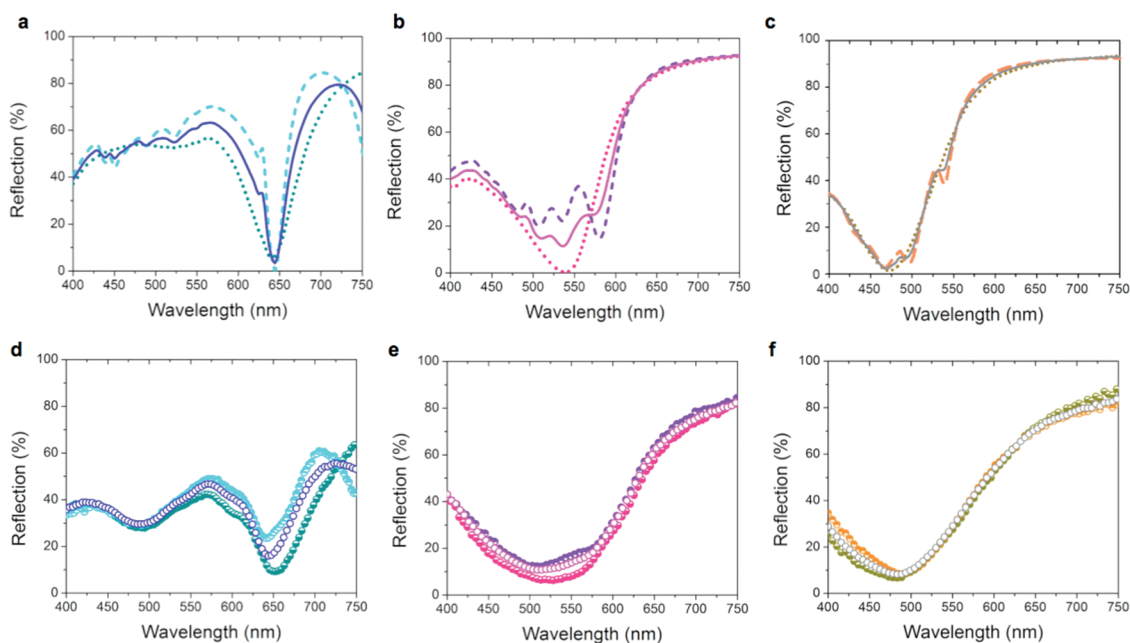
Figure 3. Color filtering behaviors in dual-function devices. (a−c) Reflection spectra calculated by RCWA simulation. Solid line, dashed line, and dotted line represent unpolarized condition, TM mode, and TE mode, respectively: (a) cyan, (b) magenta, and (c) yellow. (d−f) Measured reflection spectra. Open circle, half-down open circle, and half-up open circle represent unpolarized condition, TM mode, and TE mode, respectively: (d) cyan, (e) magenta, and (f) yellow.

Au was chosen due to its excellent conductivity and appropriate work function as an anode. The periodic Au nanograting structures were fabricated using nanoimprint lithography (NIL), followed by reactive ion etching (RIE), metal deposition, and lift-off process, to produce a large-area transparent electrode onto which OPV cells can be easily fabricated. The fabrication of the complete OPV structures using those Au nanogratings as an anode is as follows. First, the conductive PEDOT:PSS layer, often used in OPV structures as a hole-transporting layer and with the high work function for hole collecting, was cast on the Au nanograting anode. Such "composite" anode structures consisting of metallic nanogratings and PEDOT:PSS can ensure efficient hole collection and transport between the metal lines. Next, a high-performance bulk-heterojunction (BHJ)[19−24,29] photoactive layer composed of P3HT and PCBM was constructed, serving the function of converting the absorbed light to a photocurrent. After thermal annealing to optimize the BHJ nanostructures, a continuous Al cathode layer was thermally deposited. Al was selected due to its excellent performance as a cathode material for the OPV cells when combined with a thin LiF layer and cost-effectiveness.[21,30] An ultrathin 1 nm LiF was used to improve the performance of OPV cells but did not affect the optical properties of the device. The Al layer also prohibits the direct transmission of incident light.

Following the design guidelines and the fabrication processes described above, we demonstrate primary CMY colors (cyan, magenta, and yellow) under thr broadband white light condition. First, BHJ active layers of three thicknesses (90, 65 and 50 nm) were selected to control the TE polarized light to generate CMY colors, respectively. Then Au nanogratings of three corresponding periods (420, 280, and 220 nm) were selected to control the TM polarized light under the given photoactive layer thickness. In all three cases, the thicknesses of the Au nanogratings and the PEDOT:PSS layer are 40 and 30 nm, respectively. All the Au nanogratings have a ca. 0.7 duty cycle (Au line width is 0.7 of the period). The light is illuminated onto the color filter from the Au anode side, and the photograph images were taken showing distinct reflected CMY colors over large areas (Figure 1d−f). Figure 3 shows the reflection spectra of the CMY colors of the proposed structure: simulation results by rigorous coupled wave analysis (RCWA) method (upper panel) and experimental results measured by using a broadband white light source (lower panel). Clearly the expected color filtering behavior was obtained, and the experimentally measured spectra are well matched with the simulation results calculated for both polarized and unpolarized light conditions. The angle dependence of reflective filters was also tested by calculating the color variations for the CMY color in the CIE 1931 color space chromaticity diagram with increasing the incident angle (Figure S1 in the Supporting Information). The experimental spectrum was further examined by changing the viewing angle between the light source and detector using a spectroscopic ellipsometer (from 0° to 60°, Figure S2 in Supporting Information). Both results demonstrated that the color variation is not so dramatic and acceptable in some ranges (<30°).

Finally photovoltaic properties of the reflective color filter devices were measured under AM 1.5 G simulated sunlight (at 100 mW cm^{-2} intensity), and the current density *versus* voltage characteristics are summarized in Figure 4. The measured PCEs for the CMY color filters are 1.55%, 0.82%, and 0.60%, respectively. The cyan-colored devices with the thickest photoactive layer (~90 nm), leading to sufficient light absorption in this structure, showed the best efficiency with the highest short circuit current density (J_{sc}) and fill factor. The magenta-colored devices having well-matched absorption near the maximum energy band of electron-donor materials P3HT, usually centered around 550 nm,[20,21,31] have comparable J_{sc} values, with the cyan-colored even with the thinner photoactive layer (~65 nm). The yellow-colored filters also successfully generated electrical power as OPV cells, even though they have reduced absorption around the energy band of the electron-donor with the thinnest photoactive layer (~50 nm) giving the lowest J_{sc}. Furthermore, we would like to point out that in our design because the metallic nanogratings simultaneously serve as the semi-transparent electrode for the solar cell, the use of wider metal lines (0.7 duty cycle) is highly desirable because they will significantly reduce the resistance of the electrode, which is essential for large-area solar cells without degrading the PCE. As an example, current OPV cells built on ITO still suffer from insufficient conductance of the transparent ITO when they are made large-area due to the voltage drop on the resistive electrode.[32] Moreover, the superior flexibility of metallic nanostructures on the flexible substrate without conductance degradation under bent conditions[33] and the applicability to large-area roll-to-roll processing[21,33] make these dual-function devices appealing for large-area flexible display applications.

As an alternative structure for a reflective color filter, the continuous flat metal film can also be employed rather than metal nanogratings. In this scheme, the whole structure acts as a simple planar Fabry−Pérot cavity and the color filtering can be realized by the Fabry−Pérot interference effect. For the normal incidence, the TE and TM illuminations within the planar Fabry−Pérot cavity are theoretically indistinguishable and the resonant wavelength is similar to the TE component within the nanograting device. However, the devices composed of continuous flat metal films instead of nanograting structures suffer from significantly low optical transmission through the continuous metal film, inducing negligible photocurrent.
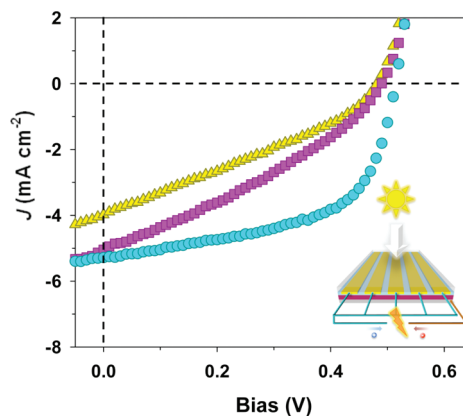
Figure 4. Photovoltaic behaviors in dual-function devices. Circle, square, and triangle symbols represent the devices showing cyan, magenta, and yellow colors, respectively. $J-V$ plots of dual-function devices. All data were measured at AM 1.5 G with an intensity of 100 mW cm^{-2}. Average solar cell characteristics such as short circuit current density (J_{sc}), open circuit voltage (V_{oc}), fill factor (FF), and power conversion efficiency (PCE) are summarized as follows: cyan (J_{sc} = 5.28 mA cm^{-2}, V_{oc} = 0.51 V, FF = 57.5%, PCE = 1.55%); magenta (J_{sc} = 5.04 mA cm^{-2}, V_{oc} = 0.49 V, FF = 33.1%, PCE = 0.82%); yellow (J_{sc} = 3.98 mA cm^{-2}, V_{oc} = 0.48 V, FF = 31.2%, PCE = 0.60%). The inset image is a schematic of a dual-function device showing photovoltaic property.

Furthermore, most of the devices tend to have an almost short circuit behavior, which is still under investigation.

Another interesting aspect of our design is that the longitudinal thickness of the photonic color filter is less than 200 nm, which is about 2 orders of magnitude thinner than that of traditional colorant-based ones. This is very attractive for the design of ultrathin colored devices.

CONCLUSIONS

In summary, we demonstrated reflective color filtering elements that simultaneously integrate the OPV function into a single device. The light absorbed by the color filter, which is otherwise totally wasted, is harvested by the OPV to generate photocurrents. The dual-function devices, which are expected to lead to higher efficiency, are currently under investigation according to the design principles suggested in this paper. Considering the scalability of OPV devices to large areas, the unique energy-generating property of the dual-functional color filters may lead to more energy-efficient e-media. The dual functionality can find another attractive application, where decorative colored OPV panels can be envisioned for light energy conversions.

METHODS

Au Nanograting Fabrication. Three types of large-area Au nanogratings having different periodicities (420, 280, and 220 nm) were fabricated by NIL-based processes. NIL was performed in a Nanonex NX2000 naonoimprinter (Princeton, NJ) using a SiO$_2$ mold with a 0.7 duty cycle on a MRI-8030 resist (Microresist Technology GmbH) spin-casted on glass substrates, at a pressure of 600 psi and a temperature of 180 °C, for 5 min. After

cooling and demolding, Ti was selectively deposited on each sidewall of the imprinted grating structures by angled deposition. Ti deposited on the resist patterns induced the undercut structures during O_2 reactive ion etching, facilitating the lift-off process. O_2 RIE (20 sccm O_2, 12 mTorr chamber pressure, and 30 W bias power), deposition of 40 nm Au with 1 nm Ti using an electron-beam evaporator, and the lift-off process completed the fabrication of Au nanograting structures on a substrate.

Dual-Function Device Fabrication. Au nanogratings on glass were cleaned in acetone and isopropyl alcohol under sonication for 20 min, respectively, and treated by O_2 plasma for 60 s. Cleaned substrates were then transferred to a N_2-purged glovebox, and the filtered PEDOT:PSS (H.C. Starck, Clevios PH 500) was spin-casted onto the Au nanograting electrodes to deposit a ~30 nm thick layer, which was subsequently baked at 115 °C for 15 min. For the photoactive layer, P3HT (Rieke Metals Inc., 4002-E, ~91% regioregularity) and PCBM (American Dye Source, purity > 99.5%) were used as received, and blend solutions were prepared by dissolving both components in chlorobenzene with a 1:1 ratio by weight. The solution was stirred for ~12 h in the N_2-purged glovebox to give a homogeneous blend system and filtered using a 0.45 μm filter. The blend solution was spin-casted onto the PEDOT:PSS layer and annealed at 130 °C for 20 min. The thickness of the blend film was controlled by changing the concentration of solution (1−1.3 wt %) and the spin-coating speed (700−2000 rpm). The thickness of the organic layer was measured by a Dektek profiler. After thermal treatment, LiF (1 nm) and Al (75 nm) were deposited by thermal evaporator at a pressure of 8×10^{-7} mbar through the circular-shaped shadow masks.

Solar Cell Performance Measurements. Current *versus* voltage characteristics were measured with a Keithley 2400 system by illuminating the OPV cells with AM 1.5 G simulated sunlight using an Oriel solar simulator with an irradiation intensity of 100 mW cm^{-2}, which was calibrated by a power meter (OPHIR, Nova-Oriel) and a reference silicon solar cell.

Supporting Information Available: Figures S1 and S2 showing angle dependence of the color filters. This material is available free of charge *via* the Internet at http://pubs.acs.org.

REFERENCES AND NOTES

1. Morton, O. Solar Energy: A New Day Dawning?: Silicon Valley Sunrise. *Nature* **2006**, *443*, 19–22.
2. Snyder, G. J.; Toberer, E. S. Complex Thermoelectric Materials. *Nat. Mater.* **2008**, *7*, 105–114.
3. Cha, S. N.; Seo, J.-S.; Kim, S. M.; Kim, H. J.; Park, Y. J.; Kim, S.-W.; Kim, J. M. Sound-Driven Piezoelectric Nanowire-Based Nanogenerators. *Adv. Mater.* **2010**, *22*, 4726–4730.
4. Harbers, G.; Bierhuizen, S. J.; Krames, M. R. Performance of High Power Light Emitting Diodes in Display Illumination Applications. *J. Disp. Technol.* **2007**, *3*, 98–109.
5. Joannopoulos, J. D.; Villeneuve, P. R.; Fan, S. Photonic Crystal. *Solid State Commun.* **1997**, *102*, 165–173.
6. Joannopoulos, J. D.; Johnson, S. G.; Winn, J. N.; Meade, R. D. *Photonic Crystals: Molding the Flow of Light*, 2nd ed.; Princeton University Press, 2008.
7. Barnes, W. L.; Dereux, A.; Ebbesen, T. W. Surface Plasmon Subwavelength Optics. *Nature* **2003**, *424*, 824–830.
8. Zayats, A. V.; Smolyaninov, I. I.; Maradudin, A. A. Nano-Optics of Surface Plasmon Polaritons. *Phys. Rep.* **2005**, *408*, 131–314.
9. Ozbay, E. Plasmonics: Merging Photonics and Electronics at Nanoscale Dimensions. *Science* **2006**, *311*, 189–193.
10. Genet, C.; Ebbesen, T. W. Light in Tiny Holes. *Nature* **2007**, *445*, 39–46.
11. Lee, H. S.; Yoon, Y.-T.; Lee, S.-S.; Kim, S.-H.; Lee, K.-D. Color Filter Based on a Subwavelength Patterned Metal Grating. *Opt. Express* **2007**, *15*, 15457–15463.
12. Laux, E.; Genet, C.; Skauli, T.; Ebbesen, T. W. Plasmonic Photon Sorters for Spectral and Polarimetric Imaging. *Nat. Photon.* **2008**, *2*, 161–164.
13. Diest, K.; Dionne, J. A.; Spain, M.; Atwater, H. A. Tunable Color Filters Based on Metal-Insulator-Metal Resonators. *Nano Lett.* **2009**, *9*, 2579–2583.
14. Xu, T.; Wu, Y.-K.; Luo, X.; Guo, L. J. Plasmonic Nanoresonators for High-Resolution Colour Filtering and Spectral Imaging. *Nat. Commun.* **2010**, *1*, 59.
15. Arsenault, A. C; Puzzo, D. P.; Manners, I.; Ozin, A. G. Photonic Crystal Full-Colour Display. *Nat. Photon.* **2007**, *1*, 468–472.
16. Kolle, M.; Salgard-Cunha, P. M.; Scherer, M. R. J.; Huang, F.; Vukusic, P.; Mahajan, S.; Baumberg, J. J.; Steiner, U. Mimicking the Colorful Wing Scale Structure of the Papilio Blumei Butterfly. *Nat. Nanotechnol.* **2010**, *5*, 511–515.
17. Cao, L.; Fan, P.; Barnard, E. S.; Brown, A. M.; Brongersma, M. L. Tuning the Color of Silicon Nanostructures. *Nano Lett.* **2010**, *10*, 2649–2654.
18. Zhao, X.; Meng, G.; Xu, Q.; Han, F.; Huang, Q. Color Fine-Tuning of CNTs@AAO Composite Thin Film Ciaisotropically Etching Porous AAO before CNT and Color Modification by Water Infusion. *Adv. Mater.* **2010**, *22*, 2637–2641.
19. Coakley, K. M.; McGehee, M. D. Conjugated Polymer Photovoltaic Cells. *Chem. Mater.* **2004**, *16*, 4533–4542.
20. Li, G.; Shrotriya, V.; Huang, J.; Yao, Y.; Moriarty, T.; Emery, K.; Yang, Y. High-Efficiency Solution Processable Polymer Photovoltaic Cells by Self-Organization of Polymer Blends. *Nat. Mater.* **2005**, *4*, 864–868.
21. Park, H. J.; Kang, M.-G.; Ahn, S. H.; Guo, L. J. Facile Route to Polymer Solar Cells with Optimum Morphology Readily Applicable to Roll-to-Roll Process without Sacrificing High Device Performances. *Adv. Mater.* **2010**, *22*, E247–E253.
22. Chen, H.-Y.; Hou, J.; Zhang, S.; Liang, Y.; Yang, G.; Yang, Y.; Yu, L.; Wu, Y.; Li, G. Polymer Solar Cells with Enhanced Open-Circuit Voltage and Efficiency. *Nat. Photon.* **2009**, *3*, 649–653.
23. Kang, M.-G.; Park, H. J.; Ahn, S. H.; Xu, T.; Guo, L. J. Toward Low-Cost, High-Efficiency, and Scalable Organic Solar Cells with Transparent Metal Electrode and Improved Domain Morphology. *IEEE J. Sel. Top. Quantum Electron.* **2010**, *16*, 1807–1820.
24. Chen, L.-M.; Hong, Z.; Kwan, W. L.; Lu, C.-H.; Lai, Y.-F.; Lei, B.; Liu, C.-P.; Yang, Y. Multi-Source/Component Spray Coating for Polymer Solar Cells. *ACS Nano* **2010**, *4*, 4744–4752.
25. Kang, M.-G.; Guo, L. J. Nanoimprinted Semitransparent Metal Electrodes and Their Application in Organic Light Emitting Diodes. *Adv. Mater.* **2007**, *19*, 1391–1396.
26. Kang, M.-G.; Xu, T.; Park, H. J.; Luo, X.; Guo, L. J. Efficiency Enhancement of Organic Solar Cells Using Transparent Plasmonic Ag Nanowire Electrodes. *Adv. Mater.* **2010**, *22*, 4378–4383.
27. Zia, R.; Selker, M. D.; Catrysse, P. B.; Brongersma, M. L. Geometries and Materials for Subwavelength Surface Plasmon Modes. *J. Opt. Soc. Am. B* **2004**, *21*, 2442–2446.
28. Dionne, J. A.; Sweatlock, L. A.; Atwater, H. A.; Polman, A. Plasmon Slotwaveguides: Towards Chip-Scale Propagation with Subwavelength-Scale Localization. *Phy. Rev. B* **2006**, *73*, 035407.
29. Yu, G.; Gao, J.; Hummelen, J. C.; Wudl, F.; Heeger, A. J. Polymer Photovoltaic Cells: Enhanced Efficiencies *via* a Network of Internal Donor-Acceptor Heterojunctions. *Science* **1995**, *270*, 1789–1791.
30. Brabec, C. J.; Shaheen, S. E.; Winder, C.; Sariciftci, N. S.; Denk, P. Effect of LiF/Metal Electrodes on the Performance of Plastic Solar Cells. *Appl. Phys. Lett.* **2002**, *80*, 1288.
31. Sunderberg, M.; Inganas, O.; Stafstrom, S.; Gustafsson, G.; Sjogren, B. Optical Absorption of Poly(3-alkylthiophenes) at Low Temperatures. *Solid State Commun.* **1989**, *71*, 435–439.
32. Lungenschmied, C.; Dennler, G.; Neugebauer, H.; Sariciftci, S. N.; Glatthaar, M.; Meyer, T.; Meyer, A. Flexible, Long-Lived, Large-Area, Organic Solar Cells. *Sol. Energy Mater. Sol. Cells* **2007**, *91*, 379–384.
33. Kang, M.-G.; Park, H. J.; Ahn, S. H.; Guo, L. J. Transparent Cu Nanowire Mesh Electrode on Flexible Substrates Fabricated by Transfer Printing and Its Application in Organic Solar Cells. *Sol. Energy Mater. Sol. Cells* **2010**, *94*, 1179–1184.